Simplified Modeling of Hybrid Soft Robots with Constant Stiffness Assumption

*Umer Huzaifa[1], Dimuthu D. K. Arachchige[1], Muhammad Aneeq uz Zaman[2], and Usman Syed[3]

***Abstract*— Soft robots have shown their value as alternatives or supplements to rigid robots in applications like search and rescue missions and complex precise tasks. Their ability to take on various shapes and apply adaptable force gives them an advantage over stiff robots. However, sometimes their soft structure doesn't offer enough force for the task. Hybrid soft robots (HSRs) combine a soft body with a stronger backbone to handle tasks needing more strength. This rigid part lets us use rigid body dynamics to estimate HSR behavior. Here, we introduce a simplified N-link rigid body dynamic model with constant stiffness to mimic HSR behavior. While soft robots' stiffness varies, the backbone in HSRs makes it similar to having constant stiffness. Comparing experiments supports the effectiveness of our N-link model for HSR modeling.**

***Index Terms*— Dynamics, hybrid soft robot, rigid body approximation.**

I. Introduction

Continuum arms are effective solutions that have proven their potential in adaptability, compliance, and safe collaboration with humans [1], [2]. Continuum arms are inspired by biological creatures and appendages such as snakes [3], octopus arms [4], and elephant trunks [5]. These robots mainly made of soft and elastic material generate motion via structural deformation (i.e., elongating, contracting, and bending) and are thus able to achieve complex poses that are more suitable to operate in unstructured environments [6].

Pneumatic muscle actuators (PMAs) are used to power human-scale continuum robotic arms in handling large objects [7]. PMAs are widely used in continuum arms due to several advantages such as ease of design and fabrication, cost of fabrication, and high power-to-weight ratio [8]. To date, a majority of continuum arms have been made of multiple sections with each comprising typically three variable-length PMAs. For effective object manipulation tasks, the strength of the continuum arm is critical. However, the compliant PMAs offer limited structural strength and as a result, they are subjected to undesirable deformations that are hard to model and may cause unstable poses (i.e., buckling) causing to reduce in the payload capacities.

Inspired by the structure of a spider monkey tail, the work reported in [9] shows an inextensible hybrid continuum arm that was designed and fabricated using a highly articulable rigid backbone and PMAs. Due to the antagonistic muscle triplets surrounding the backbone, the new fixed-length continuum arm is both compliant and able to generate a much higher stiffness range suitable for both safe and high-payload manipulation. In a different vein, authors in [10] have fabricated soft robots that are hybrid in nature by embedding rigid skeletons inside soft materials. Furthermore, the study presented in [11] demonstrates the creation of multi-material hybrid mechanisms that utilize pneumatic power and adaptive strain-limiting layers based on electrostatic adhesion. Leveraging the unique characteristics of the hybrid design, those robots have been successfully employed in grasping, manipulation, and locomotion [12]–[15].

The dynamics of continuum arms help accurately predict arms' behavior. To date, several dynamic modeling techniques have been proposed [16]. The principle of virtual power (Kane's method) was used in [17] to model the dynamics of tendon-driven continuum arms. In [18], [19], the dynamics of tendon-driven inextensible continuum arms were modeled using Cosserat rod theory. Renda et al. in [20] proposed an alternative discrete Cosserat approach that discretizes the continuous Cosserat model by assuming a piecewise constant strain along the soft arm. The advantage of this model over the continuous one is taking into account shear and torsional deformations. In [21], the Cosserat method was extended to model combined bending and twisting deformations of variable-length PMA-powered continuum arms. A real-time Cosserat-based numerical approach for the forward dynamics of soft and continuum arms was also presented in [22].

Dynamic models that are based on Lumped models such as those reported in [23]–[25] approximate the deformation of continuum arms to many segments. It leads to accurate and smooth deformation modeling but suffers from a complicated modeling approach and also losing the energy balance of the total segments. Due to large deformations continuum arms experience, the relative position, orientation, and linear and angular velocities between any pair of points along the body of these robots vary. Therefore, energy-based approaches such as the Lagrangian method have been utilized to derive equations of motion (EoM) thereof [26], [27].

A. Problem Statement

There has been an increase in interest in hybrid robots due to their superior exploration capabilities as well as safety implications for human-robot interaction. But dynamic modeling of hybrid robots has proved to be a particularly hard

[1]School of Computing, Jarvis College of Computing and Digital Media, DePaul University, Chicago, IL 60604, USA.
[2]Department of Mechanical Engineering, University of Illinois at Urbana-Champaign, Urbana, IL 61801, USA.
[3]Department of Electrical Engineering, University of Illinois at Urbana-Champaign, Urbana, IL 61801, USA.
*Corresponding author: mhuzaifa@depaul.edu

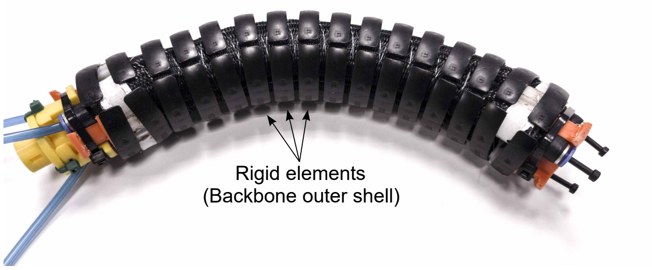

Fig. 1. Hybrid soft robot prototype at a deformed pose [9]

problem due to the unconventional construction of the robot and the inherent difficulty of modeling compliant mechanisms. The state-of-the-art approaches involve kinematic modeling-based techniques as well as open-loop control. We aim to formulate a dynamic model for a hybrid soft robot (HSR) using first principles so that the dynamic model effectively approximates the characteristics of the robot while also being computationally fast and robust.

In this work, we focus on the Hybrid Soft Robot (HSR) proposed in our previous work [9], whose physical details are provided in Table I. Its design incorporates both soft and stiff elements. The HSR as shown in Fig. 1 is essentially composed of two components; (1) pneumatic muscle actuators that control the deformation, and (2) an outer shell backbone that provides the rigidity for the HSR. This hybrid construction ensures the compliant nature of the robot while also allowing the structural robustness required for practical load-bearing tasks such as object manipulation and locomotion. Furthermore, the hybrid fixed-length construction allows for the decoupling between the stiffness and deformation control as detailed in [28]. This point is essential in obtaining an accurate and computationally fast dynamic model of the robot. Our goal is to provide an accurate kinetic and kinematic model of the HSR which is computationally tractable.

B. Why Does this Work Matter?

Planning for a desired task or a movement in a soft robot is a non-trivial task due to the uncertainty surrounding the continuum structure of the robot. In search and rescue operations, for example, if such a robot is deployed to traverse the rubble and locate a survivor, it may not be enough to use kinematic planning because the uneven terrain may not be traversable unless a required amount of torque is supplied. This is achievable if we have an approximate, fast-to-compute dynamics model at our disposal.

Other applications related to this dynamic modeling include the use of the soft arm as a supporting structure for locomotion by human users. In such applications, having a fixed structure only has a limited range of angles to impart forces on the ground. But working with a flexible stick structure like the given soft arm, we can apply force at a variation of bending ranges. Hence, overall this work helps utilize the HSR in meaningful applications.

TABLE I. Physical details of the unactuated hybrid soft robot [9].

Parameter	Value
Initial length	$L = 24\ cm$
Outer diameter	$d = 4\ cm$
Bending limit	$\phi = [0, 180°]$
Bending stiffness range	$K_b = [0, 4]\ Nmrad^{-1}$
Damping coefficient range	$K_e = [0, 1600]\ Nm^{-1}$
Weight (without pneumatic tubes)	$m = 0.15\ kg$

II. Proposed Method

In this section, we propose a dynamic model for the HSR prototype in [9]. Due to the rigidly-linked articulate construction of the backbone of the robot, we propose a constant-stiffness N-link dynamic model of the robot. This model as shown in Fig. 2b, is comprised of N rigid uniform links connected via friction-less joints involving rotational springs and dampers. The mass of the robot along with the stiffness and damping properties of the robot are uniformly distributed over the N-links in the dynamic model. As we increase N the approximation error between the dynamic model and the HSR prototype will decrease but at the cost of increasing computational complexity. This dynamic model is also quite useful as N-link manipulators have been widely studied in literature and used in practical applications. We start by describing the constant stiffness component of the dynamic model.

A. Constant Stiffness Model

By analyzing the pressure vs bending stiffness mapping of the HSR given in Table II in [9], it is apparent that the stiffness properties of the HSR are dependent on the effective pressures P_1 and P_2. This dependence is due to the fact that there are two sources of stiffness in the HSR. The first source is the stiffness in the backbone which is constant and the second source is the stiffness in the PMAs which varies in tandem with the pressure supplied to them i.e., a PMA under high pressure will be stiffer compared to one under low pressure.

Variable stiffness of HSR introduces two problems, (1) this causes the over-actuation in the HSR (stiffness/bending angle is controlled by two inputs P_1 and P_2) and (2) simulating variable stiffness manipulators is computationally expensive. To solve these problems we first observe that the relationship between bending stiffness K_{eq} and effective pressures P_1 and P_2 have a linear dominated relationship. Hence, we fit a linear model on the stiffness vs effective pressure data provided in Table II in [9] as shown below.

$$K_{eq} = -2.594 + 0.8183P_1 + 1.415P_2 \tag{1}$$

This model is shown to have a low error. We now fix the value of stiffness K_{eq} of the HSR (ideally one which allows for the maximum range of motion, based on Table II in [9]). This solves the two aforementioned problems by (1) constraining P_1 and P_2, hence solving the over-actuation problem, and (2) fixing the stiffness of the manipulator throughout the range of its motion, allowing for fast simulation of the mechanism. Under this constant stiffness constraint, the bending angle of HSR ϕ is controlled by pressure P_1, and the pressure P_2 is determined by (1). The stiffness of the robot is constant throughout the range of HSR motion.

B. N-link Rigid Body Approximation

A robot needs to be mathematically modeled for predicting its movements over time. The modeling can be of kinematic or dynamic nature depending on the interest in finding static positions over time or the evolution of movement as a result of forces and torques applied. For the latter case, the robot can be assumed to be an approximation made up of a rigid link chain. The individual links can then be modeled using the Euler-Lagrange approach to reach equations of motion. The process requires finding the position and velocity of the individual links of the robot using established variational calculus operations.

In the proposed approximation, the system is assumed to be composed of N serial link chains with each link composed of the following (Fig. 2a: a uniformly distributed mass m, a length l, and moment of inertia I. In between the links, the joints are accompanied by a spring and damper pair with coefficients given by c and k. For this initial investigation, the system is assumed to be constrained in the XZ plane as seen in Fig. 2b where a 4-link serial chain is used to approximate the HSR.

Using the model described earlier, a spring co-efficient K_{eq} for the HSR is decided and the corresponding stiffness value k for all the links is calculated using the relation for equivalent stiffness for springs in series:

$$\frac{1}{K_{eq}} = \frac{1}{k_1} + \frac{1}{k_2} + \ldots + \frac{1}{k_N}$$

and since all the individual links are similar, we can define $k_1 = k_2 = \ldots = k_N$, resulting in the following:

$$k_i = NK_{eq}$$

Consider the following dynamics for an n-link serial manipulator approximating the hybrid soft robot:

$$\frac{d}{dt}\left(\frac{\partial T}{\partial \dot{q}_i}\right) - \frac{\partial T}{\partial q_i} + \frac{\partial R}{\partial \dot{q}_i} + \frac{\partial U}{\partial q_i} = \tau \;\; i = 1, 2, \ldots, N \quad (2)$$

where $q_i \in \mathbb{R}^n$ and $\dot{q}_i \in \mathbb{R}^n$ represent the angular position and angular velocities of the joints of the robot. T represents the total kinetic energy, U represents the total potential energy and R represents the dissipation function of the torsional dampers. $\tau \in \mathbb{R}^n$ is the virtual input torque of the system. As mentioned in Sec. II, approximated model of HSR consists of N-links of mass m_i with a torsional spring and damper at its joints. Additionally, we assume a virtual torque control device at each joint. The N links each of mass m_i contributes toward the kinetic and potential energies

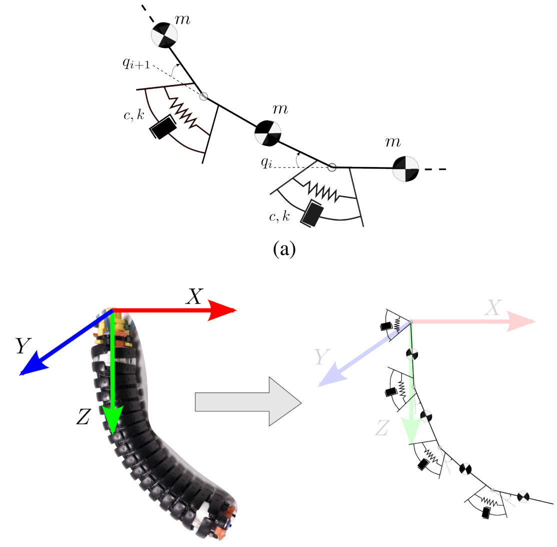

Fig. 2. (a) A single approximation unit for the soft robot. The HSR is approximated as a serial link chain of masses with springs and dampers placed in parallel at the joints. As a result, the forces acting on the adjacent links are the torques resulting from the pressures and the reaction forces from the spring and damper; (b) a soft robot arm approximated as a series of 4 links.

of the system while the torsional springs with stiffness k_i contribute towards the potential energy of the system. The dissipation function for the torsional dampers at each link is given by $0.5c_i\dot{q}_i^2$ where c_i represents the damping coefficient of the torsional damper at joint i.

The informative model of (2) can be transformed into the following control-oriented model:

$$M(q)\ddot{q} + C(q, \dot{q})\dot{q} + G(q) = \tau + \Gamma \quad (3)$$

where, M, C, and G, represent matrices for Inertia, Centrifugal forces and gravitational forces terms, and Γ represents the non-conservative forces resulting from the dampers at each virtual joint. Given the structure of the system, we end up with a useful and simple structure in the model of the system. The model in (3) can be used to design feedback control laws for following reference trajectories. The control input $\tau = \begin{bmatrix} \tau_1 & \tau_2 & \cdots & \tau_n \end{bmatrix}^T$ designed to follow the reference trajectory can be easily translated to the pneumatic pressures used in the control of HSR prototype using $\tau = K\phi$ and ϕ.

The goal is to approximate the robot as a serial link robot with spring and damper elements to reflect the stiffness characteristics of the robot. The damper element makes sure to eliminate indefinite movements that are obviously not possible in the actual robot system. The movement of the robot can provide us with information about the position of a few points on the body and the pressure inputs.

We want to use the pressure inputs to estimate the unit torques (torques at the endpoints of each mass-spring-damper unit) by using the geometry of the robot.

Following are the steps to follow for achieving this:

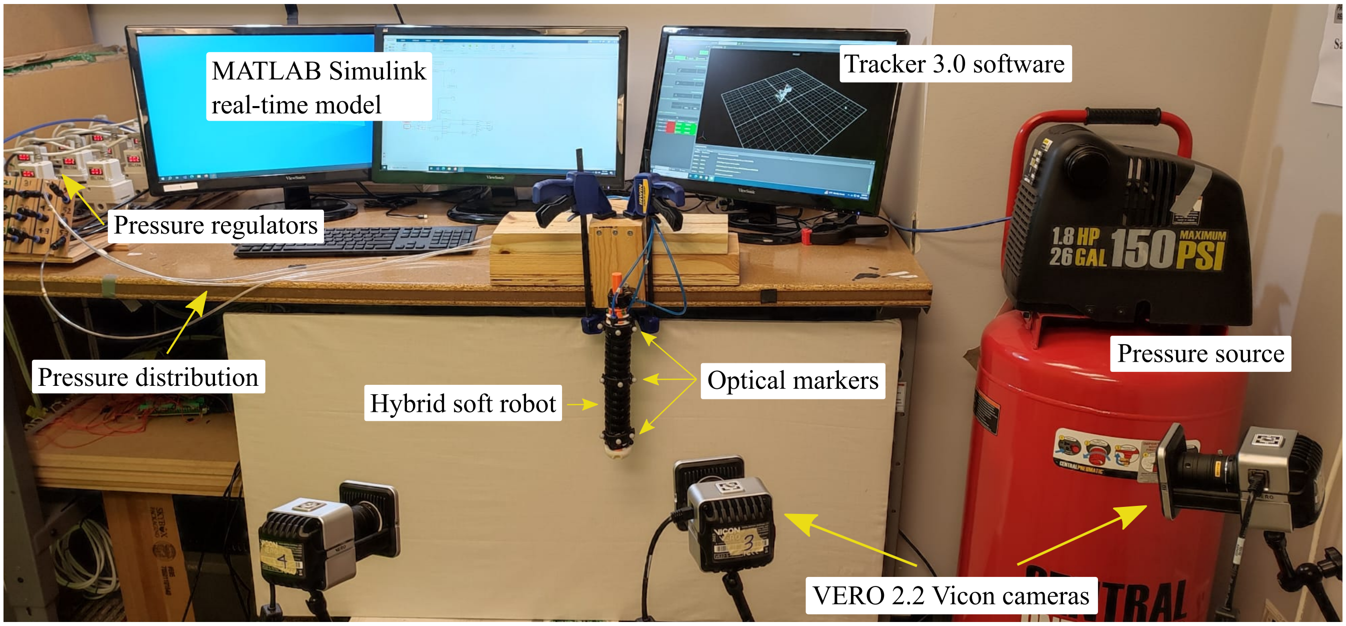

Fig. 3. The robot actuation setup and optical motion capturing system.

- Decide a number ‘n‘ of rigid links to approximate the soft robot with
- Given the pressure data, compute the applied torque at the end of each mass-spring-damper unit
- Use this computed torque to find the resulting position in the rigid body model.
- Based on the deviation between model and actual robot positions, change the spring stiffness k_i and damping co-efficient c_i.
- Keep iterating steps 3 and 4 till a reasonable agreement between the experimental data and model data is obtained.

III. Experimental Validation

A. Hybrid Soft Robot Prototype

The HSR prototype (Fig. 1) that has the physical properties given in Table I, is made of a flexible backbone and three McKibben-type extending-mode PMAs. A PMA is fabricated using a flexible Silicone tube, braided sleeves, and pneumatic union connectors. A commercially available cable carrier (Triflex R-TRL40, Igus) acts as the rigid backbone. The robot bends in a constant curvature arc due to its inextensible backbone. The readers are referred to [9] for more details on designing and fabrication of the HSR prototype.

B. Experimental Setup

The experimental setup is shown in Fig. 3. Therein, the pneumatically actuated HSR prototype [9] is vertically fixed to a table. A 6 bar air compressor is used as the pressure source. Air to each PMA of the HSR is independently supplied through proportional pressure regulators (ITV3050, SMC Pneumatics USA). The regulators are given pressure commands as $0 - 10\ V$ voltage signals via a voltage output data acquisition card (PCI-6704, National Instruments USA) interfaced with a MATLAB Simulink Real-Time model. We measure $\{X, Y, Z\}$ – task space along the robot (1 – base, 2 – middle, 3 – tip) using an optical motion tracking system (VERO 2.2, Tracker 3.0 NL Vicon Industries, Inc) at a sampling rate of 100 Hz.

$\boldsymbol{\tau}[Nm]$	$\boldsymbol{P_1}[bar]$	$\boldsymbol{P_2}[bar]$	Bending stiffness $[Nm/rad]$
0.250	1.2868	1.8735	$K_{eq} = 1.11$
0.625	0.8127	2.1477	
1.000	0.3368	2.4218	
0.100	2.4285	2.0755	$K_{eq} = 2.33$
1.800	1.4046	2.6676	
3.500	0.3807	3.2597	

TABLE II. Pressure combinations for experiment with the fixed stiffness experiment detailed in Section III. The corresponding torque values for the whole hybrid robot arm along with the stiffness coefficients are also provided.

C. Fixed Stiffness Pressures

For a simpler rigid body model, we have ensured a constant stiffness coefficient in the robot arm as explained in Sec. II. If the pressure of any two muscle actuators is kept the same, the stiffness can be varied using the third actuator, as shown in (1). Thus, for a desired stiffness K_{eq} then, we can come up with a constraint equation between P_1 and P_2. In the following experiment, the robot arm is pressurized to emulate two stiffness coefficients: 1.11 Nm/rad and 2.33 Nm/rad. The values were chosen from [9] to provide behavior on two extremes of the stiffness.

A total of six pressure combinations were applied to the robot while following the pressure constraint and stiffness coefficient, and the spatial positions of the optical trackers

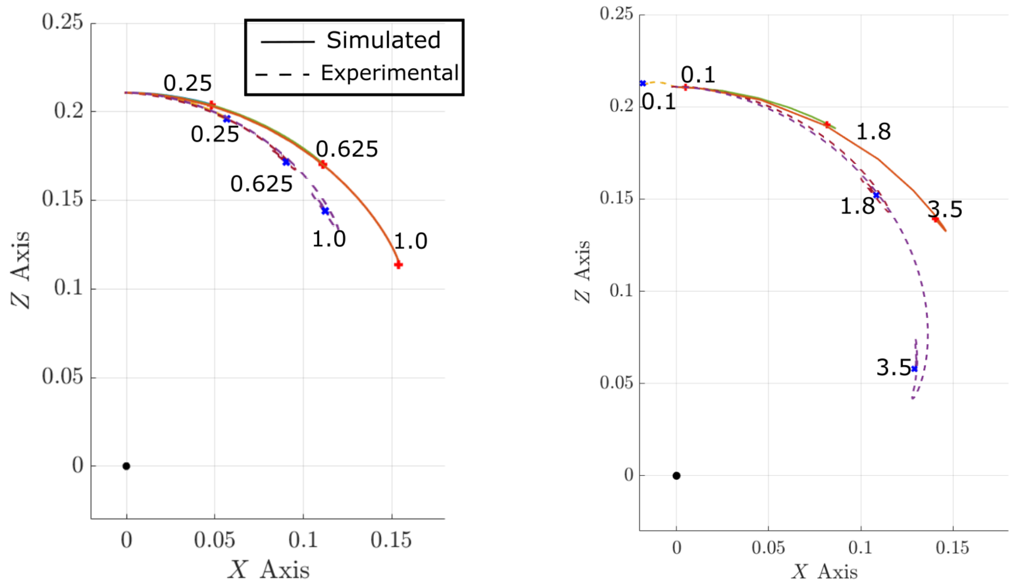

(a) (b)

Fig. 4. Movement Trajectories for the end effector of the hybrid robot arm under the pressure combinations from Table II for stiffness coefficients (a) 1.11 Nm/rad (b) 2.33 Nm/rad. The numbers indicate the overall torque applied by the hybrid robot as a result of the pressure applied in the muscle acutators.

placed at the end point of the robot were recorded as a spatial position trajectory. The spatial data was first smoothed using a moving average filter before use. The six pairs of pressure values are given in Table II.

IV. Simulation Validation and Discussion

For dynamics simulation validation of the experimental data, a conversion from the pressure combination values P_1 and P_2 need to be made to the applied torque at the joint angles between the links. First, the deflection of the robot is found from Table II in [9] by fitting a linear model over the two effective pressures P_1, P_2 and deflection angle ϕ:

$$\phi = -0.7742 - 0.2892P_1 + 0.7321P_2 \tag{4}$$

Given the deflection for the soft robot, the generated torque is given as:

$$\tau_i = \tau = K_{eq}\phi \tag{5}$$

that is, the torque applied at each of the approximating link is a function of the stiffness K_{eq} of the whole soft structure and its deflection.

In order to validate this model, the soft robot is actuated with the pressure combinations given in Table II, and the spatial trajectory of the robot is recorded. To generate a corresponding trajectory from the approximation model, a 4-link approximate model is considered with the stiffness and damping coefficients of the individual links given as $k_i = K_{eq}N$ and $c_i = C(K_{eq})N$, respectively. The value $C(K_{eq})$ was chosen using brute force for each equivalent stiffness coefficient K_{eq}. For $K_{eq} = 1.11$ Nm/rad, $C = 0.05$ Nm/rad/s was used and for $K_{eq} = 2.33$ Nm/rad, the value of C was 0.1 Nm/rad/s.

Using the torques corresponding to the applied pressures on the real system and as obtained from Eqs. 4 and 5, the trajectory from the approximate model is generated as well and the results are shared in Fig. 4. In the given comparison, the approximated system follows a circular path while the real system has a parabolic trajectory for all the tested pressure combinations. The difference becomes more prominent when the deflecting torques increase in the case of a higher stiffness coefficient for the soft robot deflection (Fig. 4b. The reason behind this dissimilarity is the existence of variable stiffness characteristic of the robot moving from its base to the tip and some hard-to-model damping effects in the hybrid robot structure. Moreover, at higher pressure values, the hybrid robot structure is deviating more from the rigid behavior thus making equal stiffness links unlikely.

From the experimental data, it seems that the robot has a varying stiffness component related to the distance from the robot base. The dynamics estimation has been carried out in a plane yet because of a relation between torque and stiffness derived from earlier work [9]. In three dimensions, however, a more direct relation will have to be derived for practical usage. Moreover, estimating the torque from pressure combinations is another source of error in the method.

V. Acknowledgement

The presented work was funded by Academic Growth and Initiative Fund (AGIF) number 602196 and Faculty Summer Research Grant from DePaul University.

VI. Conclusions

In this study, we introduced a constant stiffness N-link dynamic model tailored to a hybrid soft robot (HSR) that integrates pneumatic muscle actuators (PMAs) with an external shell backbone. Although the stiffness of the HSR flexes in response to pressure changes within the PMAs, we maintained a consistent stiffness profile by imposing a constraint relationship on the PMA pressures derived in a previous work by co-authors [9]. Based on this constraint, the deflection angle in HSR and the deflection torque was derived, and used in the pseudo-rigid body modeling of the system with torque instead of pneumatic pressures acting as the inputs at virtual joints. The approximation of pseudo-rigid body modeling was then validated through an experiment which revealed similarity in the model generated and real world robot trajectories. The comparison also reveled discrepancies in the two due to the HSR's adoption of a parabolic trajectory. Notably, these deviations become more pronounced at higher pressure values, for larger stiffness, where the constant stiffness assumption gradually loses accuracy.

Looking ahead, numerous intriguing research avenues emerge. These include refining the estimation of stiffness and damping coefficients, optimizing the number of links to balance complexity and compatibility considerations, and exploring alternative approaches like the recursive Newton-Euler method for real-time computations [29]. Furthermore, investigating force interactions between the HSR and its environment, such as ground interactions during locomotion, stands as a promising direction for further inquiry.

REFERENCES

[1] R. Qi, A. Khajepour, W. W. Melek, T. L. Lam, and Y. Xu, "Design, kinematics, and control of a multijoint soft inflatable arm for human-safe interaction," *IEEE Transactions on Robotics*, vol. 33, no. 3, pp. 594–609, 2017.

[2] A. Amaya, D. D. Arachchige, J. Grey, and I. S. Godage, "Evaluation of human-robot teleoperation interfaces for soft robotic manipulators," in *2021 30th IEEE International Conference on Robot & Human Interactive Communication (RO-MAN)*. IEEE, 2021, pp. 412–417.

[3] D. D. Arachchige, Y. Chen, and I. S. Godage, "Soft robotic snake locomotion: Modeling and experimental assessment," in *2021 IEEE 17th International Conference on Automation Science and Engineering (CASE)*. IEEE, 2021, pp. 805–810.

[4] B. Mazzolai, L. Margheri, M. Cianchetti, P. Dario, and C. Laschi, "Soft-robotic arm inspired by the octopus: Ii. from artificial requirements to innovative technological solutions," *Bioinspiration & biomimetics*, vol. 7, no. 2, p. 025005, 2012.

[5] K. Ma, X. Chen, J. Zhang, Z. Xie, J. Wu, and J. Zhang, "Inspired by physical intelligence of an elephant trunk: Biomimetic soft robot with pre-programmable localized stiffness," *IEEE Robotics and Automation Letters*, vol. 8, no. 5, pp. 2898–2905, 2023.

[6] D. B. Camarillo, C. F. Milne, C. R. Carlson, M. R. Zinn, and J. K. Salisbury, "Mechanics modeling of tendon-driven continuum manipulators," *IEEE Transactions on Robotics*, vol. 24, no. 6, pp. 1262–1273, 2008.

[7] M. A. Robertson, H. Sadeghi, J. M. Florez, and J. Paik, "Soft pneumatic actuator fascicles for high force and reliability," *Soft robotics*, vol. 4, no. 1, pp. 23–32, 2017.

[8] M. S. Xavier, C. D. Tawk, A. Zolfagharian, J. Pinskier, D. Howard, T. Young, J. Lai, S. M. Harrison, Y. K. Yong, M. Bodaghi *et al.*, "Soft pneumatic actuators: A review of design, fabrication, modeling, sensing, control and applications," *IEEE Access*, 2022.

[9] D. D. Arachchige and I. S. Godage, "Hybrid soft robots incorporating soft and stiff elements," in *2022 IEEE 5th International Conference on Soft Robotics (RoboSoft)*. IEEE, 2022, pp. 267–272.

[10] J. M. Bern, F. Zargarbashi, A. Zhang, J. Hughes, and D. Rus, "Simulation and fabrication of soft robots with embedded skeletons," in *2022 International Conference on Robotics and Automation (ICRA)*. IEEE, 2022, pp. 5205–5211.

[11] Q. Xiong, B. W. Ang, T. Jin, J. W. Ambrose, and R. C. Yeow, "Earthworm-inspired multi-material, adaptive strain-limiting, hybrid actuators for soft robots," *Advanced Intelligent Systems*, vol. 5, no. 3, p. 2200346, 2023.

[12] L. Li, F. Xie, T. Wang, G. Wang, Y. Tian, T. Jin, and Q. Zhang, "Stiffness-tunable soft gripper with soft-rigid hybrid actuation for versatile manipulations," *Soft Robotics*, vol. 9, no. 6, pp. 1108–1119, 2022.

[13] D. D. Arachchige, D. M. Perera, S. Mallikarachchi, I. Kanj, Y. Chen, and I. S. Godage, "Wheelless soft robotic snake locomotion: Study on sidewinding and helical rolling gaits," in *IEEE International Conference on Soft Robotics (RoboSoft)*, 2023, pp. 1–6.

[14] D. D. Arachchige, D. M. Perera, S. Mallikarachchi, U. Huzaifa, I. Kanj, and I. S. Godage, "Soft steps: Exploring quadrupedal locomotion with modular soft robots," *IEEE Access*, vol. 11, pp. 63 136–63 148, 2023.

[15] D. D. Arachchige, T. Varshney, U. Huzaifa, I. Kanj, T. Nanayakkara, Y. Chen, H. B. Gilbert, and I. S. Godage, "Study on soft robotic pinniped locomotion," in *IEEE/ASME International Conference on Advanced Intelligent Mechatronics (AIM)*, 2023, pp. 65–71.

[16] C. Armanini, F. Boyer, A. T. Mathew, C. Duriez, and F. Renda, "Soft robots modeling: A structured overview," *IEEE Transactions on Robotics*, 2023.

[17] Z. Liu, X. Zhang, Z. Cai, H. Peng, and Z. Wu, "Real-time dynamics of cable-driven continuum robots considering the cable constraint and friction effect," *IEEE Robotics and Automation Letters*, vol. 6, no. 4, pp. 6235–6242, 2021.

[18] D. C. Rucker and R. J. Webster III, "Statics and dynamics of continuum robots with general tendon routing and external loading," *IEEE Transactions on Robotics*, vol. 27, no. 6, pp. 1033–1044, 2011.

[19] F. Renda, M. Giorelli, M. Calisti, M. Cianchetti, and C. Laschi, "Dynamic model of a multibending soft robot arm driven by cables," *IEEE Transactions on Robotics*, vol. 30, no. 5, pp. 1109–1122, 2014.

[20] F. Renda, F. Boyer, J. Dias, and L. Seneviratne, "Discrete cosserat approach for multisection soft manipulator dynamics," *IEEE Transactions on Robotics*, vol. 34, no. 6, pp. 1518–1533, 2018.

[21] H. B. Gilbert and I. S. Godage, "Validation of an extensible rod model for soft continuum manipulators," in *2019 2nd IEEE International Conference on Soft Robotics (RoboSoft)*. IEEE, 2019, pp. 711–716.

[22] J. Till, V. Aloi, and C. Rucker, "Real-time dynamics of soft and continuum robots based on cosserat rod models," *The International Journal of Robotics Research*, vol. 38, no. 6, pp. 723–746, 2019.

[23] R. Kang, D. T. Branson, T. Zheng, E. Guglielmino, and D. G. Caldwell, "Design, modeling and control of a pneumatically actuated manipulator inspired by biological continuum structures," *Bioinspiration & biomimetics*, vol. 8, no. 3, p. 036008, 2013.

[24] I. S. Godage, R. J. Webster, and I. D. Walker, "Center-of-gravity-based approach for modeling dynamics of multisection continuum arms," *IEEE transactions on robotics*, vol. 35, no. 5, pp. 1097–1108, 2019.

[25] H. Habibi, R. Kang, I. D. Walker, I. S. Godage, and D. T. Branson, "Developing a 3-d, lumped-mass model to present behaviour of large deformation surface based continuum robots," in *IUTAM Symposium on Intelligent Multibody Systems–Dynamics, Control, Simulation*. Springer, 2019, pp. 133–147.

[26] I. S. Godage, G. A. Medrano-Cerda, D. T. Branson, E. Guglielmino, and D. G. Caldwell, "Dynamics for variable length multisection continuum arms," *The International Journal of Robotics Research*, vol. 35, no. 6, pp. 695–722, 2016.

[27] D. D. Arachchige, S. Mallikarachchi, I. Kanj, D. M. Perera, Y. Chen, H. B. Gilbert, and I. S. Godage, "Dynamic modeling and validation of soft robotic snake locomotion," in *IEEE International Conference on Control, Automation and Robotics (ICCAR)*, 2023, pp. 6–12.

[28] D. D. Arachchige, Y. Chen, I. D. Walker, and I. S. Godage, "A novel variable stiffness soft robotic gripper," in *2021 IEEE 17th International Conference on Automation Science and Engineering (CASE)*. IEEE, 2021, pp. 2222–2227.

[29] R. Featherstone, "Robot dynamics algorithms," *AIAA Journal of Guidance, Control, and Dynamics*, vol. 20, no. 2, pp. 439–448, 1997.